Additive Manufacturing 94 (2024) 104513

Contents lists available at ScienceDirect

Additive Manufacturing

journal homepage: www.elsevier.com/locate/addma

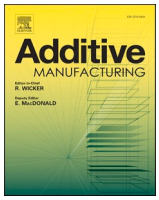

Integrated 3D printing of reconfigurable soft machines with magnetically actuated crease-assisted pixelated structures

Youchao Zhang [a], Xiaoyang Zhu [a,*], Huangyu Chen [a], Ruichen Wang [c], Siqi Qiu [b], Houchao Zhang [a], Hongke Li [a], Zhenghao Li [a], Rui Wang [a], Fan Zhang [a], Guangming Zhang [a], Yuan-Fang Zhang [b,*], Dong Wang [c,*], Hongbo Lan [a,*]

[a] Shandong Engineering Research Center for Additive Manufacturing, Qingdao University of Technology, Qingdao 266520, PR China
[c] State Key Laboratory of Mechanical System and Vibration, School of Mechanical Engineering, Shanghai Jiao Tong University, Shanghai 200240, PR China
[b] Shien-Ming Wu School of Intelligent Engineering, South China University of Technology, Guangzhou 511442, PR China

ARTICLE INFO

Keywords:
Multi-material 3D printing
Reconfigurable soft machines
Magnetic actuation
Pixelated design

ABSTRACT

Reconfigurable magnetic soft machines have a wide range of applications in soft robotics, aerospace, medical devices and flexible electronics. However, the high-precision reconfiguration of magnetically actuated soft machines is hindered by the absence of rational structural design and integrated manufacturing techniques. Here, we report an innovative design and manufacturing approach to realize magnetically actuated high-precision reconfigurability. We present a crease-assisted pixelated design using a mixture of magnetic particles and phase-change medium as the pixel points, with an elastomer as the crease to connect the pixel points, simulating origami. The design of elastomer creases improves pixel stiffness without loss of reconfigurable accuracy, thereby significantly improves the magnetic particle concentration in the pixel. An effective multi-material 3D printing technique is used to achieve the integrated printing of the designed structure. The resulting magnetically actuated soft machines exhibit remarkable capabilities, achieving small curvature bending and precise reconfiguration with weaker actuating magnetic fields (100mT). The superior performance of this design has been confirmed through demonstrations of crawling and rolling machines, magnetically controlled switches, and logic circuits. The work enhances the reconfiguration accuracy of magnetically actuated soft machines, increasing their potential for soft robotics and flexible electronics applications.

1. Introduction

Soft machines, known for their flexibility and adaptability, can meet the demands of various complex environments and diverse mission [1–4]. Among them, magnetically actuated soft machines [5–9], stand out due to their unique untethered and precise manipulation capabilities, exhibiting exceptional performance and potential. These machines have found widespread applications across diverse domains, including soft robotics [10–18], flexible electronics [19,20], medical device engineering [21–24], metamaterials [25,26], etc. By manipulating the magnetic orientation of magnetic particles, the reconfiguration of model shapes and functions can be achieved, which augments the diversity, flexibility, and adaptability of magnetically actuated soft machines. The inherent reconfigurability has positioned magnetically actuated soft machines as a focal point of recent research [27–32]. The precision of reconfiguration, as the ability to accurately control the boundaries, significantly influences the performance of the resulting applications. Enhancing reconfiguration accuracy can minimize errors and reduce the need for additional adjustments, thereby improving overall efficiency. This level of precision is crucial for ensuring precise surgical outcomes in the healthcare sector and for optimizing circuit control in flexible electronic devices. However, how to precisely alter the orientation of magnetic particles remains a crucial issue in achieving reconfigurability.

One method to achieve reconfigurable magnetically actuated soft machines involves remagnetizing the machine after heating it to the Curie temperature and applying a magnetic field during the cooling

* Corresponding authors.
E-mail addresses: zyc15056091754@163.com (Y. Zhang), zhuxiaoyang@qut.edu.cn (X. Zhu), carlchen0830@163.com (H. Chen), ruichenwang@sjtu.edu.cn (R. Wang), 2233042781@qq.com (S. Qiu), zhanghc0918@163.com (H. Zhang), lhk1164072308@163.com (H. Li), 15634218355@163.com (Z. Li), wr1970627@163.com (R. Wang), zhangfanql@163.com (F. Zhang), ustbzgm@163.com (G. Zhang), zhangyuanfang@scut.edu.cn (Y.-F. Zhang), wang_dong@sjtu.edu.cn (D. Wang), hblan99@126.com (H. Lan).

https://doi.org/10.1016/j.addma.2024.104513
Received 6 July 2024; Received in revised form 27 September 2024; Accepted 24 October 2024
Available online 26 October 2024

process [33]. However, prolonged heating inevitably causes thermal diffusion, affecting the alignment of magnetic domains adjacent to the reconfiguration region. Additionally, the shape, size, and position of the machine during the cooling process can affect the magnetic field, complicating accurate reconfiguration. A more convenient and effective solution is achieved by combining magnetic materials with phase change materials [34–37]. In this approach, the magnetic particles' orientation is free to rotate when the phase change material is in its liquid state and is locked when the change material solidifies. This method improves reconfiguration efficiency and reduces equipment requirements. While thermal diffusion does not affect the magnetic domains during reconfiguration, the phase-change material in neighboring regions can be severely disturbed, making it difficult to maintain locking in regions not intended for reconfiguration. Moreover, the deformation characteristics of the soft machine are directly influenced by its stiffness, which is limited by the particle concentration of the material. This concentration also directly impacts reconfiguration accuracy and response speed. Therefore, accurate reconfiguration still requires improved structural design and manufacturing solutions.

In this work, we present a feasible design and manufacturing approach to achieve magnetically actuated high-precision reconfigurability. The concept of 'pixelation' is proposed to efficiently partition the reconfigurable magnetically actuated machine into discrete pixel points, allowing precise independent control of the reconfiguration process. The substrate, inspired by origami techniques [38,39], employs elastomeric materials with creases connecting individual pixels, resulting in improved bending properties. Since the pixels and the fold areas are made of different materials, the performance of the machine's bending sections is no longer influenced by the stiffness of the material in the pixel area. This has allowed for the design of a magnetically actuated material with a high mass ratio of magnetic particles, up to 80 %, to serve as the actuation and basis. We developed a multi-nozzle 3D printer for the integrated manufacturing of crease-assisted pixelated machine. The direct ink writing process was used to prepare the substrates, creases, and outer frames of the pixels, while fusion deposition modeling process was used to fill the pixels with magnetic material. This composite manufacturing process ensures machine resolution while allowing for the filling of highly concentrated materials. Experimental results demonstrate that the crease-assisted pixelated, reconfigurable magnetically actuated soft machine exhibits excellent bending performance and reconfiguration accuracy. To illustrate the practical versatility of our design, we developed a range of motion-based machines, magnetic switches, and logic circuits. Compared to single-material, homogeneous reconfigurable magnetically actuated soft machines, the crease-assisted pixelated design offers improved reconfiguration accuracy while enhancing multiple performance metrics. This study advances the development of integrated additive manufacturing of structures, materials, and processes, as well as the properties of reconfigurable magnetically actuated soft machines.

2. Methods and materials

2.1. Reconfigurable magnetic materials

Anhydrous ethanol (A112717, Aladdin®, China), succinic acid (analytically pure) solution (S108855, Aladdin®, China), NdFeB particle (LW-N-400, Xinnuode Transmission Parts Co., China) and polyvinylpyrrolidone (P434440, Aladdin®, China) were mixed in a mass ratio of 200:10:5:1. The mixture was subjected to ultrasonication for 1 hour and then filtered to obtain NdFeB particle fully wrapped by PVP. Under water bath heating at 80℃, the NdFeB@ PVP and paraffin wax were mixed at a 1:1 vol ratio, which translates into a mass ratio of 80 % (±3 %) of the total mass of the material. The mixed was then ultrasonicated for 1 hour to obtain the reconfigurable magnetic material, as shown in Figure S1. The prepared material, observed under the microscope in Figure S2, exhibits excellent uniformity. The flow properties of the phase-change magnetic material were also tested, with results shown in Figure S3, indicate that it is well-suited for printing.

2.2. Preparation of the elastomer materials

PDMS (Dow Corning 184, Xike Electronics Limited, China) was used. The PDMS consists of A-glue and B-glue (hardener). For machine preparation, 20 g of A-glue was taken. The corresponding B-glue (2 g) was taken at a mass ratio of 10:1. The mixture was stirred using a magnetic stirrer for 15 minutes until homogeneous dispersion was achieved. The dispersed mixture was then placed in vacuum equipment. A vacuum pump was used to achieve a negative pressure of −1.0 kPa. The pressure was maintained for 15 minutes to remove air bubbles. The defoamed PDMS was then used for machine preparation. In our process, the elastomer, which defines the shape resolution of the machine, plays a critical role due to its rheological properties. The rheological property of the ink is a critical factor in DIW 3D printing. We conducted rheological tests on the formulated DIW ink, and the results are shown in Figure S4. Shearing disrupts the cross-linked network, thinning the ink and reducing its viscosity. However, during the printing process, the ink is subjected to shearing forces when extruded, which disrupt these structures and reduce the internal resistance of the fluid, leading to a decrease in viscosity. Consequently, inks with shear-thinning properties (pseudoplastic behavior) exhibit better adaptability during the material extrusion process [40]. The figure demonstrates that the ink used in DIW effectively exhibits shear-thinning behavior under shear force, confirming its suitability as a printing material for DIW processes. Additionally, the DIW ink (PDMS) behaves as a Newtonian fluid at low shear rates. However, it exhibits pseudoplastic behavior when the shear rate reaches a critical value, resulting in a sudden drop in viscosity.

2.3. Configuration of the sacrificial layer materials

Fill a 200 mL beaker with 90 mL of deionized water, and heat it on a heating plate set to 120°C until boiling. Then, add 4.5 g of hydroxypropyl methylcellulose (H108819, Aladdin®, China) to the boiling water and stir the solution using a magnetic stirrer until it cools down and is evenly mixed. After removing the magnetic stirrer, place the cellulose solution in a low-temperature environment to deflate any foam. Once defoamed, the solution is ready for use.

2.4. Multi-nozzle integrated printing process

Place a 100 mm × 100 mm float glass slide in a spin coater and dispense 5 mL of hydroxypropyl methylcellulose (HPMC) solution onto the center of the slide. Spin coat for 30 seconds at 2000 rpm, then dry the coated slide in a 60°C oven for 30 minutes to ensure complete moisture removal and form a dense cellulose film on the glass surface. For the direct-write pressure feed system, assemble a 5cc syringe, a 21 G (12.7 mm length, 520 μm inner diameter) stainless steel dispensing needle, an air pump, and a pressure regulator. Pour vacuum-degassed PDMS into the syringe and set the printing platform to 80°C with a nozzle-to-platform distance of 120 μm, a pressure of 0.25 kPa, and a deposition speed of 30 mm/s. Under these conditions, fabricate four layers of shape bases, each with a thickness of 100 μm. The use of 3D printing allows for high flexibility in shape design. Increase the temperature of the printing platform to 90°C and print ten layers with a speed of 30 mm/s, a nozzle acceleration of 1000 mm/s^2, and a layer height of 40 μm to create an external framework with a thickness of 400 μm and a line width of 800 μm. Next, assemble a hot-melt printing feed system consisting of a 100 cc stainless steel syringe, a 0.5 mm inner diameter Musashi nozzle, a pressure regulator, a temperature controller, and a heating barrel. Load the reconfigurable magnetically-actuated material into the syringe, maintain the printing platform at 80°C, and heat the syringe to 80°C. Set the nozzle-to-platform distance to 120 μm, the backpressure to 0.25 kPa, the deposition speed to 10 mm/s, and the

nozzle acceleration to 1000 mm/s^2 to slowly fill the pixels. After cooling, encapsulate the device using direct-write molding technology. Place the encapsulated device in a 60°C dryer for 2 hours to allow complete curing. Finally, rinse the device under running water to detach it from the float glass.

2.5. Printing parameter testing

A series of parameter measurement experiments were designed. The parameters, including pressure, printing temperature, number of print lines, number of print layers, and printing speed, all influence the formation of the pixels. Each experiment involved varying one parameter while keeping the others constant to determine its effect on the pixel formation.

2.6. Properties and preparation of conductive silver paste

The silver paste used in the experiment is NT-ST201S (NANO TOP, China). At room temperature (25°C), it has a viscosity of 35,000 ± 8000 dPa·S, a volume resistivity of ≤2mΩ·cm, an adhesion level of 4–5B, and a density of 2.4 ± 0.2 g/cm^3. The design and manufacturing process requires a pressure of 0.1 kPa and a printing speed of 5 mm/s at room temperature. The paste is then deposited and placed in a drying oven at 120°C for 1 hour to complete the curing process.

2.7. Magnetization and reconfiguration

2.7.1. Magnetization

Dongguan Nasheng Electronic Equipment Technology Co., Ltd. was commissioned to complete the magnetization of the prepared machine using their NS.15 magnetizer. The specific magnetization parameters are as follows: a magnetization voltage of DC 1500 V, an output current of 150 kA, a magnetic field strength of 3 T, a pulse duration of 10 ms, and an energy release of 4000 J, to achieve the magnetization of the machine. Since all the machines prepared by this process are reconfigurable, there is no need for regional magnetization during the magnetization process.

2.7.2. Reconfiguration

Reconfiguration can be achieved in two ways: total reconfiguration and regional reconfiguration.

Total Reconfiguration: After magnetization, the machine was placed on a heating plate at 100°C. As the temperature rises, the paraffin underwent a phase transition, causing the neodymium iron boron particles @PVP to transition from a fixed state to a free state. At this point, under the influence of an external magnetic field, the model was manually bent into the desired shape. Upon cooling, the neodymium iron boron particles @PVP within the machine once again transitioned from a free state to a fixed state. When an external magnetic field was reapplied, the machine was actuated into the desired shape under its influence. The process was repeated by placing the machine back on the 100°C heating plate. As the temperature rose again, the neodymium iron boron particles @PVP transitioned from a fixed state back to a free state, allowing for another iteration of the overall machine reconfiguration.

Regional Reconfiguration: The magnetized machine is placed on the experimental bench. A heating rod is used to heat a designated area of the machine, causing the paraffin wax in that area to undergo a phase transition. This allows the NdFeB particles @PVP to change from a fixed state to a free state. Under the influence of an external magnetic field, the NdFeB particles @PVP will align with the magnetic field. The magnetic field is then set to a specific orientation, and the heating rod is removed, allowing the designated area to cool down. As it cools, the paraffin wax solidifies, and the NdFeB particles @PVP return to a fixed state, fixing the magnetic orientation. The magnetic orientation of each area of the machine is determined as needed. The process is repeated to achieve further reconfiguration.

2.8. Performance experiment

2.8.1. bending experiment

A two-pixel machine with different crease depths was designed. The magnetic orientation of each pixel is perpendicular to the plane and opposite to each other. Both pixels were fixed in the same position and subjected to the same vertical magnetic field directed upward. A stationary camera was used to record the bending behavior of the units, and the relevant data were collected.

2.8.2. heating experiment

Three different two-pixel models with varying structures were designed. The left pixel of each model was heated, and a thermal imaging camera (TG165, FLIR Systems. USA) was used to observe and record the temperature changes in the right pixel.

2.8.3. Mechanical performance testing

The maximum tensile force and the maximum strain at failure were measured for machines with different fold depths, fold widths, and thicknesses. Additionally, multiple sets of machines were subjected to hundreds of cyclic bending cycles, after which the maximum tensile force and the maximum strain at failure were tested again.

2.9. Other devices

Syringe Pump, TYD02–02-CE, Sede Instrument Co.; Fujihara Oil-Free Vacuum Pump, Microcomputer 750D, Taizhou Qibo Tool Co., Ltd.; Insulation Board, Model 032, Langfang Hongye Thermal Insulation Material Sales Co., Ltd.; Precision Pressure Reducing Valve, RW14, Shanghai Woyuan Automatic Control Valve Co., Ltd.; Digital Constant Temperature Stirrer, Model 85–2, Changzhou Yinneng Experimental Instrument Factory; Heating Base Plate, XKDR50–600, Pengfei Hardware Electric Heating Appliances Co., Ltd.; Precision Electronic Balance, MJN-681, Ruijin Yongheng Electronic Scale Co., Ltd.; Electric Hot Air Drying Oven, DHG-903385-III, Shanghai Shengke Instrument Equipment Co., Ltd.

2.10. FEA simulation

The simulation of bending is implemented by the finite element analysis software COMSOL Multiphysics (version 6.0, COMSOL Inc., Sweden). The solid mechanics module coupled with the magnetic field without current module was used to build the FEA machine. The magnetically driven deformation at each step was analyzed by the interaction calculation of magnetic force by the magnetic field-no-current module and the interaction calculation of deformation by the solid mechanics module. The machine is meshed with a tetrahedral grid with a size range of 0.3 ~ 3 mm, and the following input parameters are used for all simulations: an applied uniform magnetic field of 150mT. A flux density of 1.2 mT is used for the magnetized region of the prototype. A user-defined element subroutine developed by Zhao et al. [41] is used to predict the magnetically actuated deformation of the machine in other part. Implemented in the commercial finite-element analysis software Abaqus 2021 (Dassault Systems, France). The simulation parameters are consistent with bending.

3. Results and discussions

3.1. Multi-nozzle printing process

We have developed a multi-nozzle 3D printer equipped with both fused deposition nozzles and DIW nozzles (illustrated in Fig. 1a and Figure S5) [42,43]. To attain reconfigurability and ensure performance during operation, we developed a magnetically responsive material with high particle content, utilizing wax as the phase-change material. Given the rheological limitations of highly concentrated phase-change

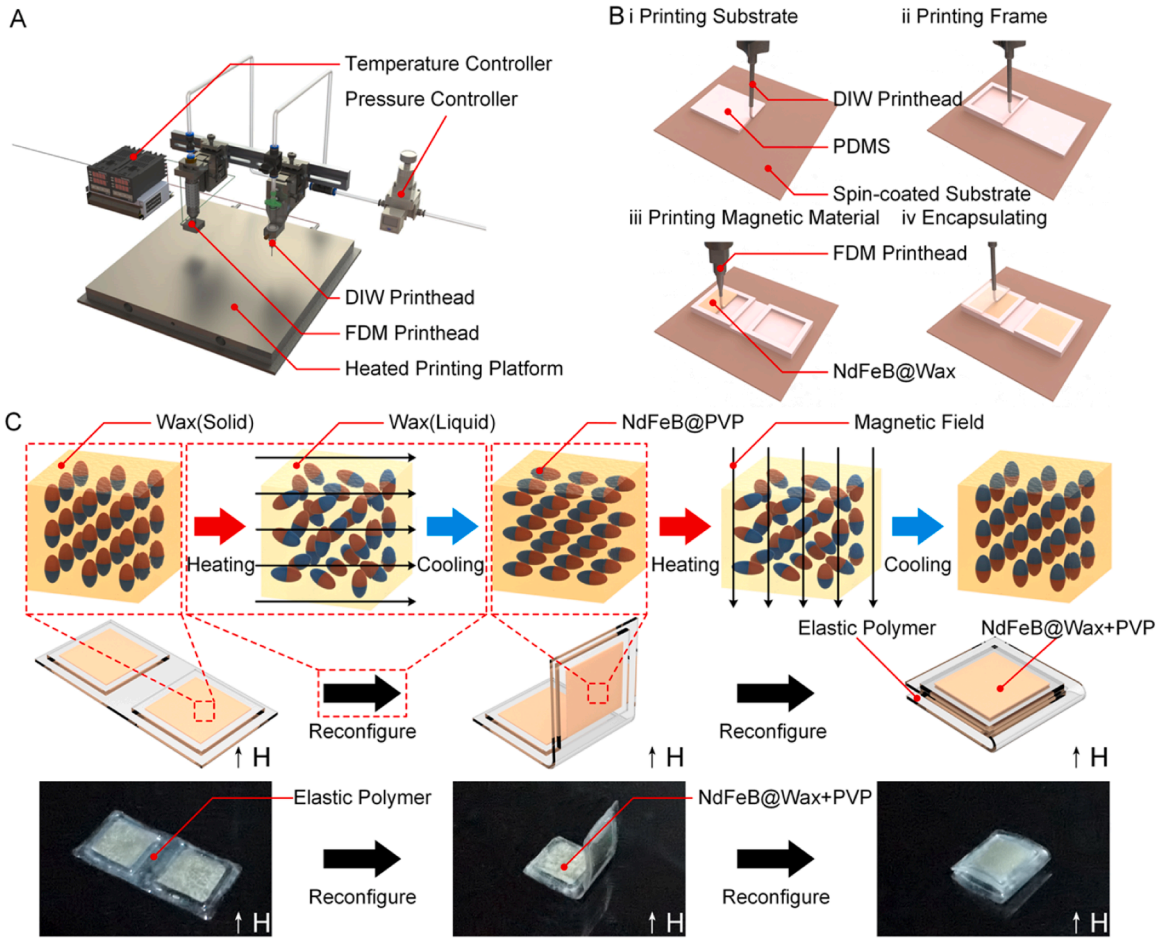

Fig. 1. Equipment, processes, and principles. (A) The printing equipment used, which integrates a DIW nozzle and a fused deposition nozzle. (B) The specific preparation process: first the substrate and the outer frame of the machine are printed by DIW, then the reconfigurable magnetic material is filled by fused deposition, and finally the encapsulation is realized by DIW. (C) The basic principle of reconfiguration: the phase change of the material is achieved by heating, the orientation of the magnetic particles within the machine is controlled by the external magnetic field, and the magnetic orientation is then fixed by the phase change. A simple two-pixel machine is prepared to validate the feasibility of the reconfiguration.

magnetic materials, and the phase-change material has a melting point of 47°C and is solid at room temperature, achieving precise printing resolution through fused deposition modeling is challenging. Therefore, we opted for a direct ink writing (DIW) process [44] to directly print the elastomer, ensuring accurate construction of the machine's substrate, crease and the outer frame of each pixel. Subsequently, a large fused deposition printhead deposits the high-particle-content magnetically responsive material within the high-resolution outer frame. This hybrid process effectively mitigates paste clogging in the fused deposition while maintaining the resolution integrity of the printed machine through DIW. To achieve precise control over the molded thickness, we manipulated the DIW nozzle without material to scrape off any protrusions resulting from the fused deposition, ensuring meticulous control over the final dimensions.

The detailed preparation process is outlined in Fig. 1b. The process begins with DIW, which deposit elastic materials onto a substrate that serves as the foundation of the machine. Next, the substrate temperature is raised to facilitate printing of each pixel's outer frame onto the substrate via DIW. Once the temperature is elevated, a high-particle-content reconfigurable magnetic material is deposited into the preformed pixel using fused deposition. Finally, the spaces are sealed with DIW, completing the fabrication.

This combination of processes ensures precise machine formation while addressing the rheological challenges associated with highly concentrated materials and nozzle obstruction. Furthermore, the use of multiple materials effectively addresses the limitations of stiffness imposed by the material concentration when driven by soft machines. Additionally, through theoretical derivations (see Supporting Text), we have established that increasing the concentration of magnetic material within the machine proportionally augments the magnetic force generated under a constant magnetic field. By elevating the concentration of magnetic material, we can reduce the required magnetic field strength, while maintaining the machine's desired actuation effect, thereby enhancing control precision and minimizing potential environmental or operational impacts of the magnetic field.

Figure S6-Figure S11 details the exploration of printing parameters, including the effects of line count, print temperature, number of print layers, print layer height, print speed and print air pressure on print results are shown separately. For the number of printed lines, increasing the number of lines can effectively improve the quality of the frame, as evidenced by the height and width of the lines. However, when the number of lines exceeds two, further increases no longer significantly enhance the height of the frame but instead affect the thickness, directly impacting the resolution. Therefore, the optimal number of lines is two. Regarding the printing temperature, increasing the temperature can accelerate the curing process and control the self-leveling effect, which influences the resolution. However, when the temperature exceeds 80°C, the material inside the nozzle is affected by thermal radiation and begins to cure slowly, leading to nozzle clogging. Hence, the printing temperature is set at 80°C.The number of layers and layer height of the

outer frame directly impact the thickness and quality of the structure. When the layer height or number of layers is too low, the internal phase-change material may not fill properly, compromising the resolution. Conversely, if the number of layers or layer height is too high, cumulative errors can affect the overall quality of the model. After considering these factors, a layer height of 4 layers with each layer being 100 μm thick is chosen. For the printing pressure, higher pressure results in proportional increases in line width and height. Depending on the requirements and design, different pressure conditions can be selected. In this study, a printing pressure of 30 kPa is chosen.

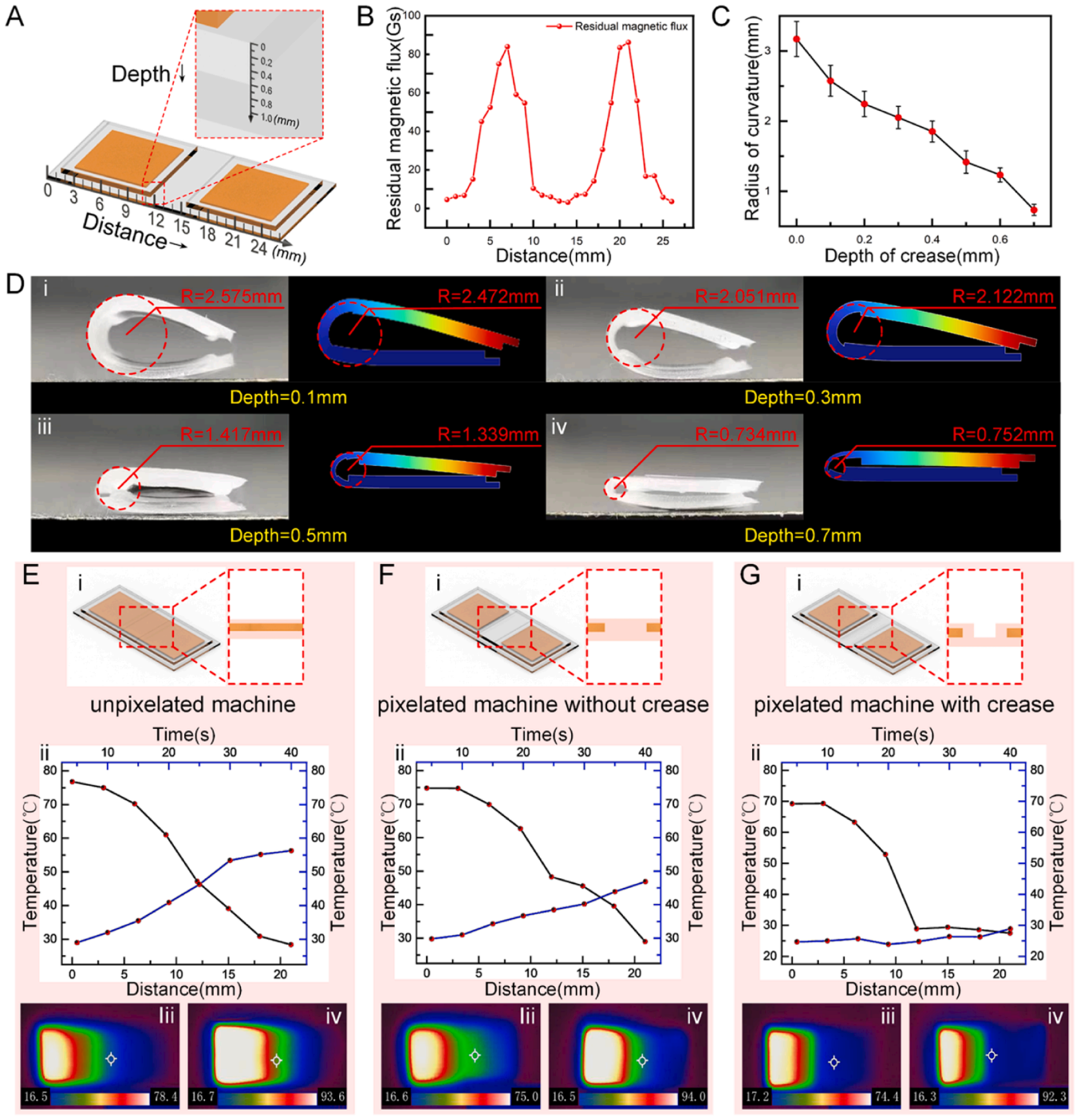

Fig. 2. Performance tests. (A) Definitions of Distance and Depth in the Machine: Distance refers to the horizontal measurement from the left end of the machine. Depth denotes the vertical measurement of the crease, extending downwards from the encapsulated surface. (B) Residual magnetic field strength distribution: illustrates the residual magnetic field strength distribution in a two-pixel machine post-magnetization. (C) Relationship between the radius of curvature and the depth of its crease. (D) compares simulation results of the machine's bending behavior at varying crease depths under a uniform magnetic field with experimental outcomes: (i) depth=0.1 mm; (ii) depth=0.3 mm; (iii) depth=0.5 mm; (iv) depth=0.7 mm; (E) Machine without pixelated design. (F) Machine featuring a crease-free pixelated design. (G) Machine incorporating both pixelated and crease designs between pixels: (i) schematic of the structure; (ii) the relationship between distance and temperature at 80°C; and the relationship between time and temperature when heated to 100°C at a distance of 15 mm; (iii) the temperature at the center of the right pixel when heated to 80°C; (iv)temperature at a distance of 15 mm at 100°C for 40 s.

3.2. Principles of reconfiguration

The basic principle of reconfiguration is illustrated in Fig. 1c. In its solid state, the phase change materials contain magnetic particles that are locked in place, referred to as the "locked state." When an external magnetic field is applied, the magnetic moments generated do not cause the particles to rotate but instead drive the entire machine, allowing for effective control and actuation by the external magnetic field. Upon heating the material to its melting point (significantly lower than the Curie temperature), the magnetic properties remain unchanged, but the magnetic particles are free to rotate within the phase change material, which is termed the "free state." The viscosity of the phase change material restricts the displacement of the magnetic particles. In this free state, when an external magnetic field is applied, the magnetic particles rotate without driving the entire machine. Once the particles are oriented as desired, cooling the system causes the phase-change material to solidify, thereby locking the particles in place again. The material thus transitions back from the free state to the locked state, achieving magnetic reconfiguration. The relationship between temperature and the reconfiguration response is shown in Figure S12. When the same model is reconfigured at different temperatures and then subjected to the same magnetic field, it can be observed that the rearrangement of the magnetic direction only occurs above 70℃. Furthermore, effective reconfiguration to achieve the desired outcome is only realized when the temperature is above 90℃. This process can be repeated to achieve multiple reconfigurations.

3.3. Results of performance testing and optimization

A series of bending experiments were conducted to validate the crease-assisted pixelated structure's ability to induce bending performance. To achieve this, two-pixel machines with varying crease thicknesses between pixels were carefully designed and tested (Fig. 2a). Magnetic flux residual testing, combined with a Gaussian counter, was used to perform a detailed analysis of the machines. The collected data was averaged and presented visually on a line chart (Fig. 2b), revealing a consistent pattern in the residual magnetic flux distribution directly influenced by the pixel configuration. Notably, the two pixels within the machine rearranged themselves in opposite orientations when exposed to an external magnetic field, creating a perpendicular orientation to the plane. The COMSOL simulation tool was employed to understand this behavior further. This allowed for the creating of various machines and applying magnetic fields to study their effects more closely. Comparing the simulation results, one significant finding was that the depth of the crease separating the pixels had a profound impact on the overall bending effect (Fig. 2c). As the crease depth increase, the curvature radius decreased proportionally (Fig. 2d). In fact, the machine with the deepest crease exhibited a radius of curvature that was only one-sixth of that of a machine without any crease. These results not only confirmed the effectiveness of the crease-assisted pixelated structure in enhancing bending performance but also highlighted the improved quality of the bend achieved.

To assess the precision of pixelized structure reconfiguration, we tested three designs: machine without pixelated design (Fig. 2e), crease-free two-pixel (Fig. 2f), and creased two-pixel (Fig. 2g). As expected, the un-pixelated machine quickly approached paraffin wax's melting point (47°C), indicating a reconfiguration impact. The crease-free pixelated machine stayed cooler but still neared the melting point. However, the creased machine showed no such effect, with only the left pixel heated and the right pixel remaining below the melting point. Next, we magnetically reconfigured the right pixel of all three machines in the opposite orientation under the same magnetic field. The un-pixelated machine bent, with some influence on the right pixel. The crease-free pixelated machine bent less, showing a smaller bending region and more controlled reconfiguration. The crease-assisted pixelated machine bent as intended, with the right pixel unaffected by the reconfiguration. These results indicate that the crease-assisted pixelated structure design significantly enhances reconfiguration accuracy and overall effect. Details of the heating conditions can be found in Figure S13-Figure S18.

Figure S19-Figure S22 for performance tests. The effects of crease width, model thickness, and crease depth on tensile properties and fatigue testing were tested. The impact of increasing fold depth on the curvature radius and the maximum tensile force that can be withstood was calculated and is shown in Figure S23. When the fold depth increases from 400 μm to 500 μm, the reduction rate of the curvature radius is only 4.4 %, which is lower than the reduction rates observed when the fold depth increases from 300 μm to 400 μm (17.7 %) and from 200 μm to 300 μm (17.4 %). However, the maximum tensile force decreases by 27 % when the fold depth increases from 400 μm to 500 μm, which is greater than the reductions observed when the fold depth increases from 300 μm to 400 μm (20.2 %) and from 200 μm to 300 μm (17.3 %). Considering both the mechanical performance and the bending behavior, a fold depth of 400 μm is deemed optimal for an 800 μm machine. Figure S24 explains the response speed of the machine, highlighting the unique advantages of magnetic actuation in soft machines. Figure S25 provides the results of cyclic experiments under the same configuration and magnetic field conditions, as well as the cyclic testing results of the machine undergoing repeated reconfigurations, ensuring the reliability and stability of the machine's formation.

3.4. Multiple configs of single machine

Using the aforementioned principles, we designed and created a hollow cross (Figure S26 and Video S1), a hollow square (Figure S27 and Video S2), and a simple mesh structure (Figure S28 and Video S3), each with three distinct magnetic distributions. In conjunction with the simulation results, three different reconfiguration results are realized. The experimental results closely matched the simulations, confirming the machine's reliability and strong reconfigurability, even at low magnetic field strengths, thanks to a high magnetic particle mass ratio. Expanding the number of pixels can tangibly enhance the diversity of reconfigurable shapes. In this study, a machine comprising 16 pixels (Fig. 3a and Video S4) has been devised. Initially, the magnetic machine's orientation is disordered and erratic. The initial magnetic direction is related to the magnetization process. Heating reconfigures specific pixels, causing the machine's magnetic field along the diagonal to divide into two regions with opposite orientations (Fig. 3b config. 1). This leads to a diagonal folding of the machine under the influence of an upward-perpendicular magnetic field. The individual machine pixels were reconfigured to divide the machine into two regions of opposing magnetic properties along the central line (Fig. 3b config. 2). Under the effect of a magnetic field directed vertically upwards, the machine exhibits folding along its centerline. By repeating the above steps and constantly modifying the orientation of the magnetic domains within each pixel of the machine, while simultaneously applying a magnetic field that acts upwardly perpendicular to the plane, diverse types of actuations were achieved. Shovel-shaped deformations were achieved by bending the two corners of the machine (Fig. 3d). Arch-bridge-shaped distortions were achieved by bending along the central line (Fig. 3e). Tunnel-shaped distortions were achieved by bending along the diagonal (Fig. 3f), and distortions similar to four-pointed stars were produced by bulging the center (Fig. 3g). The simulation of the six deformation modes have been compared with experimental results. The experimental results align with the simulation results. The results above confirm the exceptional reconfigurability properties of this process.

Supplementary material related to this article can be found online at doi:10.1016/j.addma.2024.104513.

3.5. Simulation of multiple motion modes of a single machine

To investigate the applicability of a crease-assisted pixelated reconfigurable magnetically actuated soft machines in soft robotics, we

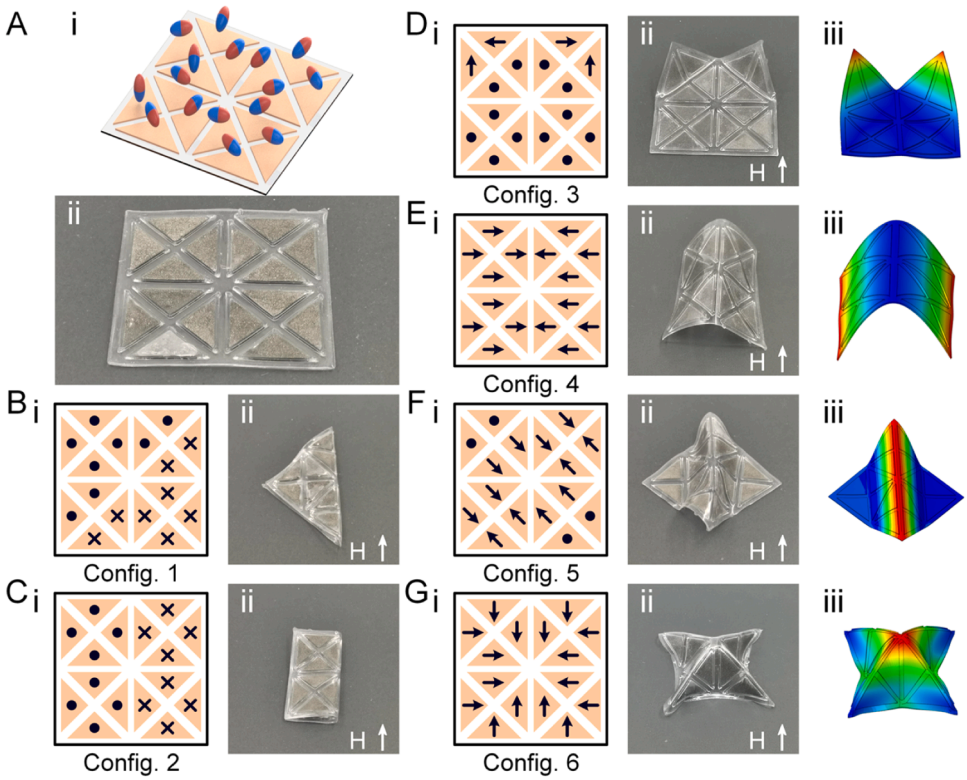

Fig. 3. Reconfiguration validation of the 16-pixel machine (A) the physical figure of the 16-pixel machine (The magnetic properties of the particles are disordered in the initial state); (B) config 1: folding along the center line; (C) config 2: folding along the diagonal line; (D) config 3: spade deformation; (E) config 4: arch bridge deformation; (F) config 5: tunnel deformation; (G) config 6: four-pointed star-like deformation: (i) magnetic distribution; (ii) actual drive effect; (iii) simulation results.

designed a series of three-pixel motion machines showcasing various motion modes. We then evaluated the effectiveness of these machines through two distinct programming modes, verifying their exceptional motion capabilities. Firstly, the magnetic orientations of the machines were aligned parallel through reprogramming (Fig. 4a). Subsequently, the machines underwent rapid tumbling under the influence of the external magnetic field (Figure S29). Each tumble had a width equivalent to the machine's body length. Moreover, the rate of movement was directly proportional to the speed of the magnetic field underneath. By altering the magnetic domain orientation of the magnetic material inside the machine (Fig. 4b), it was possible to reset the machine from tumbling to crawling. The crease between the pixels effectively increased the distance of a single movement due to the crease-assisted pixelated design, with every application and withdrawal of the magnetic field resulting in the machine crawling up to 1/3 of its body length. A displacement equivalent to one body length of the machine can be accomplished every three cycles of magnetic field application and withdrawal, as shown in Figure S30. Refer to Video S5. We also examined the impact of different crease shapes on the movement of machines in the presence of a magnetic field. Machines without creases exhibit a smaller bending angle and a shorter movement distance, equivalent to 1/6 of the body length. The findings efficiently showcase that crease-assisted pixelated structural design enhances movement efficiency, resulting in swift and efficient motion.

Supplementary material related to this article can be found online at doi:10.1016/j.addma.2024.104513.

3.6. Reconfiguration in magnet switches

Magnetically actuated elastomers possess flexible properties, and reprogrammability offers diverse applications. This section focuses on the potential of reconfigurable magnetically actuated soft machines equipped with flexible electronics, which achieve reconfigurable magnetic switches [45]. A multi-joint, four-pixel magnetic actuated soft switch was designed (Fig. 5a), along with the corresponding LED light array (Fig. 5b). The development of a reconfigurable switch featuring four pixels and multiple joints is noteworthy due to its ability to enable position control through selective reconfiguration of different regions, much like the motion of a finger bending its joints in a straight line to reach a specific point. Following machine preparation, an electrical area is created by printing silver paste on the relevant area of the "fingertip"(The device is shown in the Fig. 5c). The preparation process is described in Fig Figure S31 and Figure S32. Through the effect of the magnetic field, constant reconfiguration results in different arrangements of the magnetic domain orientations, achieving different connections of the circuits. First, the machine is heated to reset the magnetism of each reconfigurable region of the machine perpendicular to the plane (Fig. 5d). Subsequently, a perpendicular magnetic field is applied upwards to the plane, and the machine remains stationary. At this stage, the opposite end of the circuit is held on, resulting in the lighting of LED 1. After that, the machine is heated in an upwardly perpendicular magnetic field and bent into the necessary shape to light LED 2 (Fig. 5e). After being cooled to room temperature in the magnetic field, the field is withdrawn, and the machine is restored to its initial state. LED 1 remains lit. When a magnetic field is applied perpendicularly upwards to the plane, this configuration of magnetic domains causes the machine to reconfigure, which in turn causes the bending and finally causes LED 2 to light up. Repeat the above steps for the third programming mode (Fig. 5f). Before the magnetic field is applied, LED 1 remains lit; as the strength of the magnetic field is progressively increased perpendicularly to the plane upwards, the machine bends, LED 2 lights up and then goes out, and finally, LED 3 lights up and remains lit. By observing (Figure S33) and recording the current of the DC power supply (Figure S34), this design demonstrates the capability of

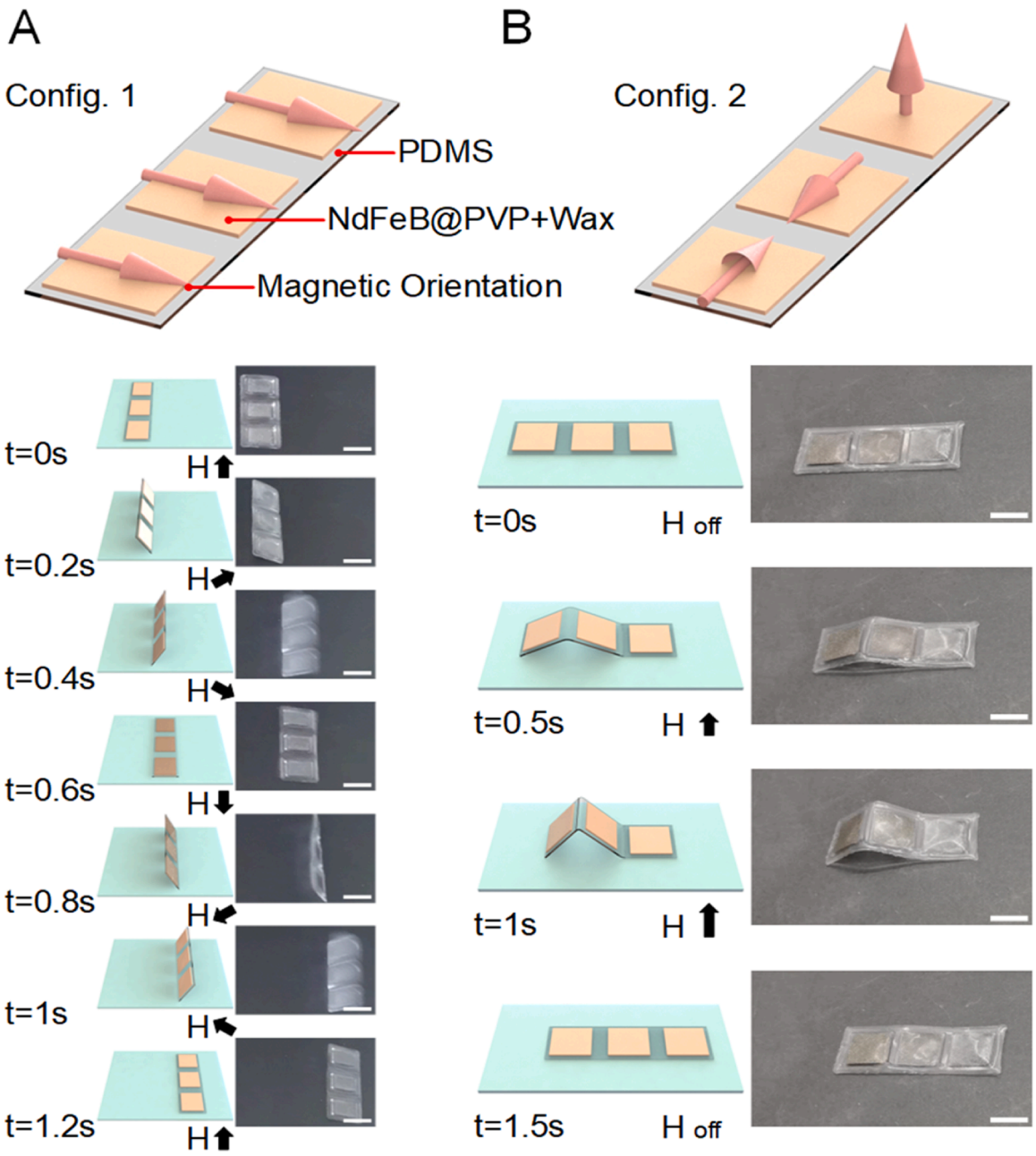

Fig. 4. Demonstration of the movement effects of the pixel (A) tumbling mode; (B) crawling mode. The direction and strength of the magnetic field during actuation and the actual movement effect (scale: 10 mm).

being reconfigured and the potential for integration with flexible electronics. This experiment demonstrates the efficiency of the reconfiguration method. Further research could increase the speed of temperature rise and fall to achieve faster reconfiguration with potential applications in flexible electronics, wireless multifunctional robots, and other fields.

3.7. Reconfiguration in logic circuit

Based on the magnetic switch, this section presents the design and preparation of a magnetic actuated reconfigurable logic circuit. The preparation process is described in Figure S35. We have fabricated seven fundamental logic circuits (the structure is as shown in the Fig. 6a. This section specifies that magnetic domains pointing upwards perpendicular to the plane in the magnetic controlled domain are identified as 0, and those pointing downwards are identified as 1. Also, specify that the output signal is 1 when the LED is illuminated and 0 when the LED is off.

The first logic circuit is the NOT circuit (Fig. 6b and Video S6). The magnetic domain orientation of the machine is reset perpendicular to the plane upwards by the first heating, i.e., the magnetic region is reset to 0. At this point, the external magnetic field is applied perpendicular to the plane upwards, the magnetic region is not driven, the LED remains lit, and the output signal is 1. After the fixation of the machine, heat the magnetic area with the effect of the magnetic field perpendicular to the plane downwards. Remove the heat source and allow the machine to cool to room temperature before removing the constraint. The input signal of the magnetic region is 1, and the machine is free again. At this point, apply the magnetic field perpendicular to the plane upwards again, and the magnetic region is folded, the circuit is disconnected, the LED turns off, and the output signal is 0. This implements the NOT logic circuit, (0) → 1, (1) → 0. Using this as a foundation, we extended the machine's reconfigurable region (i.e., the number of signal input regions) to 2. As a result, we could design and fabricate the remaining six

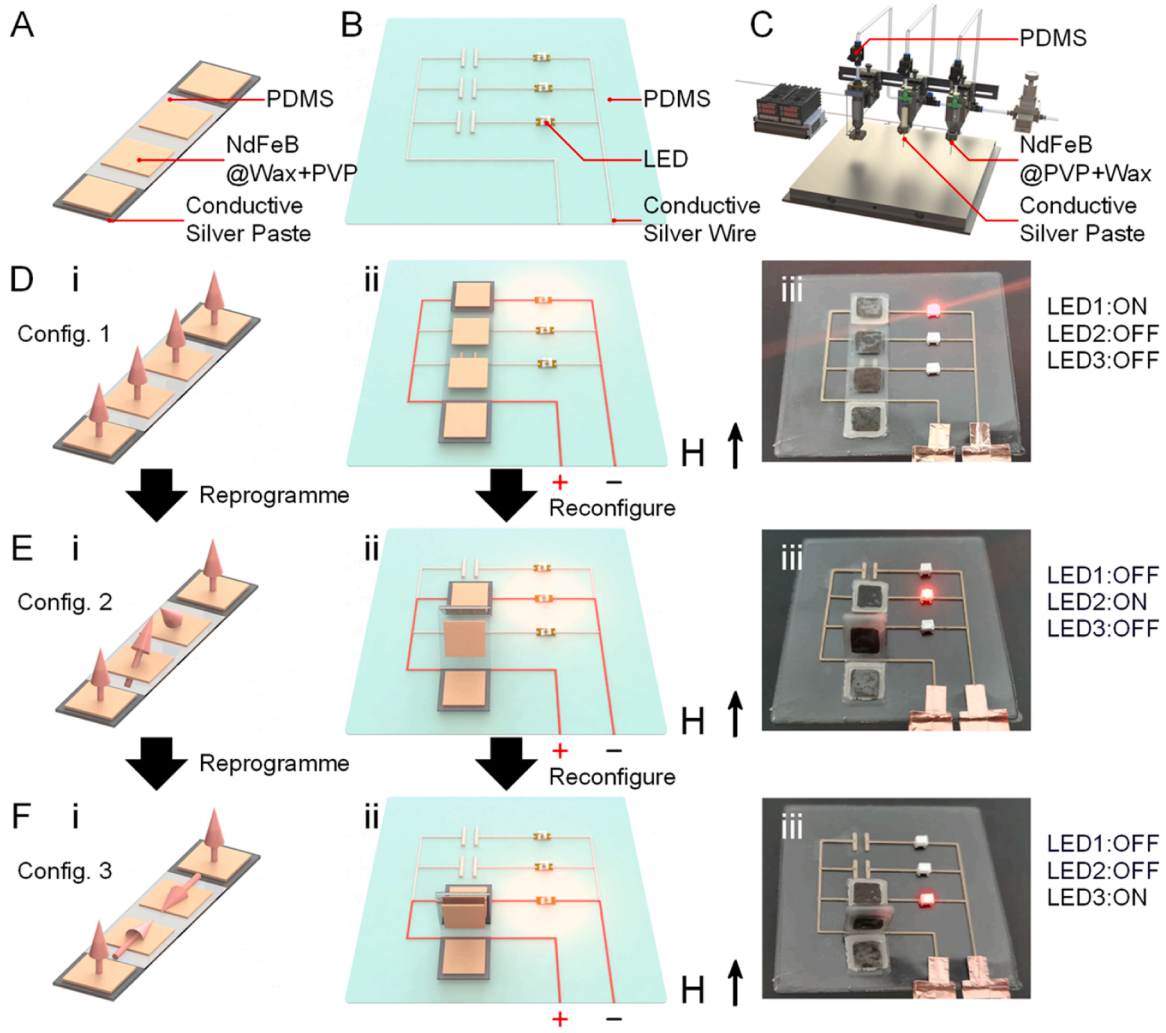

Fig. 5. Machine design of the magnetic switch. (A) Schematic of the machine; (B) schematic of the parallel switching array; (C) equipment used for preparing; (D) config 1: first LED lit (E) config 2: second LED lit (F) config 3: third LED lit: (i) magnetic distribution; (ii) model of actuated result; (iii) actual effect of magnetic drive.

logic circuits. Taking the AND circuit (Fig. 6c and Video S7) as an example, we begin with both magnetic pixels having perpendicular magnetism to the upward-facing plane, indicating an input signal of (0, 0). On applying the magnetic field vertically upwards to the plane, the magnetic pixels remain stationary, and the LED remains unilluminated, resulting in an output signal of 0. Next, we reconfigure the two magnetic pixels to introduce an input signal of (0, 1), leading to the displacement of one pixel when the magnetic field is applied. After the movement, the LED remains unlit, and the output signal remains at 0. The same result is witnessed once the input signal is altered to (1, 0). Modify the input signal to (1,1), actuate both pixels, activate the circuit, illuminate the LED, and ensure the output signal is 1. This method guarantees proper command of the input signal and feedback of the output signal for the AND circuit, in which (0,0) →0, (0,1) →0, (1,0) →0, and (1,1) →1. Following the above principle, the remaining basic logic circuits were designed simultaneously, and the input signal control and output signal feedback were implemented using reconfigurable magnetic machines: OR logic circuit (Fig. 6d and Video S8): (0,0)→0, (0,1)→1, (1,0)→1, (1,1)→1; NOR logic circuit (Fig. 6e and Video S9): (0,0)→1, (0,1)→0, (1,0) → 0, (1,1) → 0; NAND logic circuit (Fig. 6f and Video S10): (0,0) → 1, (0,1) → 1, (1,0) → 1, (1,1) → 0; XOR logic circuit (Fig. 6g and Video S11): (0,0) → 0, (0,1) → 1, (1,0) → 1, (1,1) → 0; XNOR logic circuit (Fig. 6h and Video S12): (0,0)→1, (0,1)→0, (1,0)→0, (1,1)→1. The logic circuits' current variations were monitored during the reconfiguration of the circuit, along with the signal inputs and outputs (Figures Figure S36-Figure S42). The combination of logic circuits and reconfigurable magnetic actuators expand the applications of magnetic actuators and lays the foundation for their use in flexible electronics and related industries.

Supplementary material related to this article can be found online at doi:10.1016/j.addma.2024.104513.

4. Conclusion

By blending Neodymium Iron Boron (NdFeB) particles with paraffin wax, we have developed a composite material that serves as the source of driving force, the basis for reconfiguration, and the constituent of the pixels. Polydimethylsiloxane (PDMS), the crease substrate connecting individual pixels, ensures excellent tensile and bending properties. The varying stiffnesses of the pixel and crease result in a significant increase in the magnetic particle content of the material, while maintaining drive performance. A 3D printer based on the Direct Ink Writing (DIW) and Fused Deposition Modeling processes has been developed to facilitate the integrated fabrication of the crease-assisted pixelated machinery. Experimental results demonstrate that the designed crease-assisted pixelated, reconfigurable magnetically-actuated soft machine exhibits superior bending performance and reconfiguration accuracy. The effectiveness of the crease-assisted pixelated design was validated through applications in motion models, magnetically-controlled switches, and logic circuits. This design not only ensures

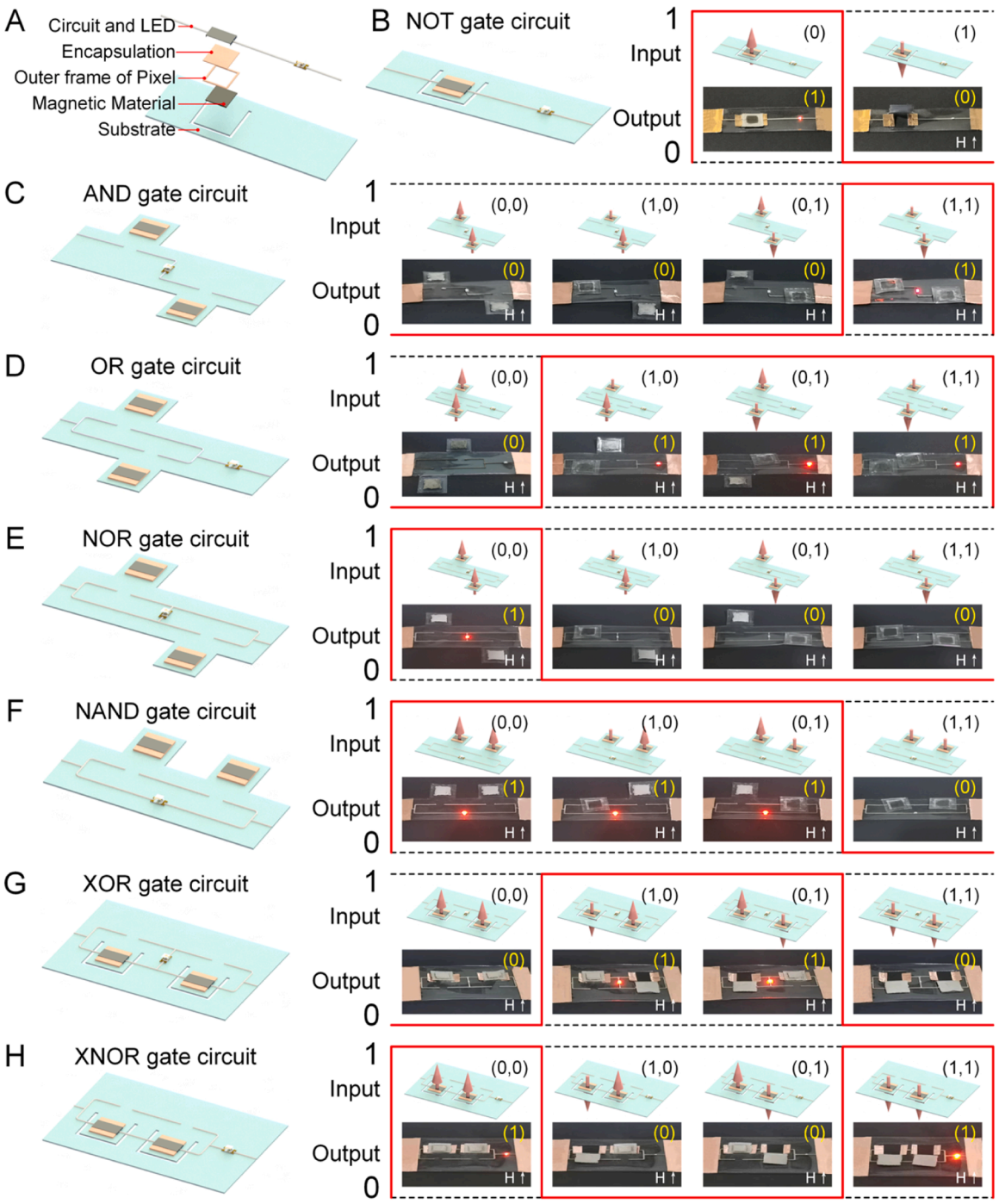

Fig. 6. Design of logic circuits (A) Exploded view of a logic circuit; (B) NOT circuits: (0)→1, (1)→0; (C) AND logic circuits: (0,0)→0, (0,1)→0, (1,0)→0 and (1,1)→1; (D) OR logic circuits: (0,0)→0, (0,1)→1, (1,0)→1, (1,1)→1; (E) NOR logic circuit: (0,0)→1, (0,1)→0, (1,0)→0, (1,1)→0; (F) NAND logic circuit: (0,0)→1, (0,1)→1, (1,0)→1, (1,1)→0; (G) XOR logic circuit: (0,0)→0, (0,1)→1, (1,0)→1, (1,1)→0; (H) XNOR logic circuit: (0,0)→1, (0,1)→0, (1,0)→0, (1,1)→1.

reconfiguration accuracy but also effectively guarantees bending performance and maintains high particle concentration. As a result, the motion efficiency of the machine is improved, and the requirement for external magnetic fields during operation is reduced, bringing remarkable control precision and efficiency, particularly beneficial for soft robotics applications. Furthermore, magnetic switch control is achieved through folding rather than bending, offering a more precise and controllable alternative. This folding approach simplifies the machine's design while increasing the effective contact area of the folded surfaces, which is highly advantageous for flexible circuits.

The prospects for future research directions are highly promising. Using variable stiffness materials as the skeleton, flexible circuits as the controller, and the central processor clock cycle as the time node for reconfiguration and driving, it is possible to develop a fully remote reconfigurable soft machine that can reconfigure, actuate, and control models using only a magnetic field. Additionally, the integration of high-density, micro-scale designs and functional gradient thermal insulation materials could enable complex functions in thermally sensitive environments, offering significant potential for applications in medical and other microenvironments. Furthermore, the crease-assisted pixelated design presents opportunities to adapt to various stimuli such as light, electricity, and heat. This versatility demonstrates the potential for

widespread application in different fields and industries.

In conclusion, this paper presents a crease-assisted pixelated reconfigurable magnetic actuated soft machine combining a multi-nozzle integration process. This approach improves the reconfiguration accuracy of reconfigurable magnetically actuated soft machines in terms of process, design and materials, and improves the bending and response properties. The feasibility of application, convenient reconfiguration, and rapid response of the crease-assisted pixelated, reconfigurable machine is demonstrated across three applications. Furthermore, subsequent considerations include increasing the pixelated integration degree, reducing the pixel size, and effectively enhancing the pixel's design. This study advances the development of integrated additive manufacturing of structures, materials, and processes, as well as the properties of reconfigurable magnetically actuated soft machines.

CRediT authorship contribution statement

Hongbo Lan: Writing – review & editing, Supervision. **Ruichen Wang:** Software. **Dong Wang:** Writing – review & editing. **Xiaoyang Zhu:** Writing – review & editing, Supervision. **Yuan-Fang Zhang:** Writing – review & editing, Supervision. **Youchao Zhang:** Writing – original draft, Methodology, Data curation, Conceptualization. **Guangming Zhang:** Writing – review & editing. **Hongke Li:** Funding acquisition. **Houchao Zhang:** Writing – review & editing. **Siqi Qiu:** Software. **Huangyu Chen:** Software, Investigation, Data curation. **Fan Zhang:** Writing – review & editing. **Rui Wang:** Formal analysis. **Zhenghao Li:** Funding acquisition.

Declaration of Competing Interest

The authors declare that they have no known competing financial interests or personal relationships that could have appeared to influence the work reported in this paper.

Acknowledgments

This study was supported by National Natural Science Foundation of China (Grant No. 52375348 and 52175331), the Natural Science Foundation of Shandong Province, China (Granted No. ZR2022ME014 and ZR2020ZD04).

Appendix A. Supporting information

Supplementary data associated with this article can be found in the online version at doi:10.1016/j.addma.2024.104513.

Data Availability

Data will be made available on request.

References

[1] M. Schaffner, J.A. Faber, L. Pianegonda, P.A. Rühs, F. Coulter, A.R. Studart, 3D printing of robotic soft actuators with programmable bioinspired architectures, Nat. Commun. 9 (2018) 878, https://doi.org/10.1038/s41467-018-03216-w.
[2] Y. Zhang, N. Zhang, H. Hingorani, N. Ding, D. Wang, C. Yuan, B. Zhang, G. Gu, Q. Ge, Fast-Response, Stiffness-Tunable Soft Actuator by Hybrid Multimaterial 3D Printing, Adv. Funct. Mater. 29 (2019) 1806698, https://doi.org/10.1002/adfm.201806698.
[3] O.A. Araromi, M.A. Graule, K.L. Dorsey, S. Castellanos, J.R. Foster, W.-H. Hsu, A. E. Passy, J.J. Vlassak, J.C. Weaver, C.J. Walsh, R.J. Wood, Ultra-sensitive and resilient compliant strain gauges for soft machines, Nature 587 (2020) 219–224, https://doi.org/10.1038/s41586-020-2892-6.
[4] Y.-F. Zhang, Z. Li, H. Li, H. Li, Y. Xiong, X. Zhu, H. Lan, Q. Ge, Fractal-Based Stretchable Circuits via Electric-Field-Driven Microscale 3D Printing for Localized Heating of Shape Memory Polymers in 4D Printing, ACS Appl. Mater. Interfaces 13 (2021) 41414–41423, https://doi.org/10.1021/acsami.1c03572.
[5] Y. Kim, X. Zhao, Magnetic Soft Materials and Robots, Chem. Rev. 122 (2022) 5317–5364, https://doi.org/10.1021/acs.chemrev.1c00481.
[6] G.Z. Lum, Z. Ye, X. Dong, H. Marvi, O. Erin, W. Hu, M. Sitti, Shape-programmable magnetic soft matter, Proc. Natl. Acad. Sci. 113 (2016), https://doi.org/10.1073/pnas.1608193113.
[7] J. Zhang, Y. Guo, W. Hu, M. Sitti, Wirelessly Actuated Thermo- and Magneto-Responsive Soft Bimorph Materials with Programmable Shape-Morphing, Adv. Mater. 33 (2021) 2100336, https://doi.org/10.1002/adma.202100336.
[8] X. Kuang, S. Wu, Q. Ze, L. Yue, Y. Jin, S.M. Montgomery, F. Yang, H.J. Qi, R. Zhao, Magnetic Dynamic Polymers for Modular Assembling and Reconfigurable Morphing Architectures, Adv. Mater. 33 (2021) 2102113, https://doi.org/10.1002/adma.202102113.
[9] R. Wang, J. Wang, Z. Zhu, D. Wang, Multimodal Magnetic Soft Robots Enabled by Bistable Kirigami Patterns, IEEEASME Trans. Mechatron. (2024) 1–12, https://doi.org/10.1109/TMECH.2024.3379979.
[10] J. Wang, D. Wang, L. Dong, M. Zhang, G. Gu, Analytical Modeling and Inverse Design of Centimeter-Scale Hard-Magnetic Soft Robots, IEEE Trans. Autom. Sci. Eng. (2024) 1–12, https://doi.org/10.1109/TASE.2023.3313395.
[11] Z. Huang, G. Shao, D. Zhou, X. Deng, J. Qiao, L. Li, 3D printing of high-precision and ferromagnetic functional devices, Int. J. Extrem. Manuf. 5 (2023) 035501, https://doi.org/10.1088/2631-7990/acccbb.
[12] C. Ma, S. Wu, Q. Ze, X. Kuang, R. Zhang, H.J. Qi, R. Zhao, Magnetic Multimaterial Printing for Multimodal Shape Transformation with Tunable Properties and Shiftable Mechanical Behaviors, ACS Appl. Mater. Interfaces 13 (2021) 12639–12648, https://doi.org/10.1021/acsami.0c13863.
[13] H. Wang, Z. Zhu, H. Jin, R. Wei, L. Bi, W. Zhang, Magnetic soft robots: Design, actuation, and function, J. Alloy. Compd. 922 (2022) 166219, https://doi.org/10.1016/j.jallcom.2022.166219.
[14] Y. Li, Z. Qi, J. Yang, M. Zhou, X. Zhang, W. Ling, Y. Zhang, Z. Wu, H. Wang, B. Ning, H. Xu, W. Huo, X. Huang, Origami NdFeB Flexible Magnetic Membranes with Enhanced Magnetism and Programmable Sequences of Polarities, Adv. Funct. Mater. 29 (2019) 1904977, https://doi.org/10.1002/adfm.201904977.
[15] W. Hu, G.Z. Lum, M. Mastrangeli, M. Sitti, Small-scale soft-bodied robot with multimodal locomotion, Nature 554 (2018) 81–85, https://doi.org/10.1038/nature25443.
[16] Q. Ze, S. Wu, J. Nishikawa, J. Dai, Y. Sun, S. Leanza, C. Zemelka, L.S. Novelino, G. H. Paulino, R.R. Zhao, Soft robotic origami crawler, Sci. Adv. 8 (2022) eabm7834, https://doi.org/10.1126/sciadv.abm7834.
[17] Z. Xu, Y. Chen, Q. Xu, Spreadable Magnetic Soft Robots with On-Demand Hardening, Research 6 (2023) 0262, https://doi.org/10.34133/research.0262.
[18] J. Wang, R. Wang, Z. Zhu, K. Zhou, D. Wang, Untethered kirigami soft robots with programmable locomotion, Appl. Phys. Rev. 10 (2023) 041405, https://doi.org/10.1063/5.0155355.
[19] Y. Zhao, S. Gao, X. Zhang, W. Huo, H. Xu, C. Chen, J. Li, K. Xu, X. Huang, Fully Flexible Electromagnetic Vibration Sensors with Annular Field Confinement Origami Magnetic Membranes, Adv. Funct. Mater. 30 (2020) 2001553, https://doi.org/10.1002/adfm.202001553.
[20] Z. Qi, M. Zhou, Y. Li, Z. Xia, W. Huo, X. Huang, Reconfigurable Flexible Electronics Driven by Origami Magnetic Membranes, Adv. Mater. Technol. 6 (2021) 2001124, https://doi.org/10.1002/admt.202001124.
[21] X. Zhang, J. Ai, Z. Ma, Y. Yin, R. Zou, B. Su, Liquid Metal Based Stretchable Magnetoelectric Films and Their Capacity for Mechanoelectrical Conversion, Adv. Funct. Mater. 30 (2020) 2003680, https://doi.org/10.1002/adfm.202003680.
[22] Y. Kim, H. Yuk, R. Zhao, S.A. Chester, X. Zhao, Printing ferromagnetic domains for untethered fast-transforming soft materials, Nature 558 (2018) 274–279, https://doi.org/10.1038/s41586-018-0185-0.
[23] A. Ramos-Sebastian, S. Gwak, S.H. Kim, Multimodal Locomotion and Active Targeted Thermal Control of Magnetic Agents for Biomedical Applications, Adv. Sci. 9 (2022) 2103863, https://doi.org/10.1002/advs.202103863.
[24] B. Wang, K.F. Chan, J. Yu, Q. Wang, L. Yang, P.W.Y. Chiu, L. Zhang, Reconfigurable Swarms of Ferromagnetic Colloids for Enhanced Local Hyperthermia, Adv. Funct. Mater. 28 (2018) 1705701, https://doi.org/10.1002/adfm.201705701.
[25] S.M. Montgomery, S. Wu, X. Kuang, C.D. Armstrong, C. Zemelka, Q. Ze, R. Zhang, R. Zhao, H.J. Qi, Magneto-Mechanical Metamaterials with Widely Tunable Mechanical Properties and Acoustic Bandgaps, Adv. Funct. Mater. 31 (2021) 2005319, https://doi.org/10.1002/adfm.202005319.
[26] B. Wang, C. Xu, G. Duan, W. Xu, F. Pi, Review of Broadband Metamaterial Absorbers: From Principles, Design Strategies, and Tunable Properties to Functional Applications, Adv. Funct. Mater. 33 (2023) 2213818, https://doi.org/10.1002/adfm.202213818.
[27] Z. Wang, K. Wang, D. Liang, L. Yan, K. Ni, H. Huang, B. Li, Z. Guo, J. Wang, X. Ma, X. Tang, L. Chen, Hybrid Magnetic Micropillar Arrays for Programmable Actuation, Adv. Mater. 32 (2020) 2001879, https://doi.org/10.1002/adma.202001879.
[28] J. Cui, T.-Y. Huang, Z. Luo, P. Testa, H. Gu, X.-Z. Chen, B.J. Nelson, L. J. Heyderman, Nanomagnetic encoding of shape-morphing micromachines, Nature 575 (2019) 164–168, https://doi.org/10.1038/s41586-019-1713-2.
[29] F.H. Zhang, Z.C. Zhang, C.J. Luo, I.-T. Lin, Y. Liu, J. Leng, S.K. Smoukov, Remote, fast actuation of programmable multiple shape memory composites by magnetic fields, J. Mater. Chem. C. 3 (2015) 11290–11293, https://doi.org/10.1039/C5TC02464A.
[30] J. Zhang, Y. Guo, W. Hu, R.H. Soon, Z.S. Davidson, M. Sitti, Liquid Crystal Elastomer-Based Magnetic Composite Films for Reconfigurable Shape-Morphing Soft Miniature Machines, Adv. Mater. 33 (2021) 2006191, https://doi.org/10.1002/adma.202006191.
[31] B. Zou, Z. Liang, D. Zhong, Z. Cui, K. Xiao, S. Shao, J. Ju, Magneto-Thermomechanically Reprogrammable Mechanical Metamaterials, Adv. Mater. 35 (2023) 2207349, https://doi.org/10.1002/adma.202207349.

[32] J. Kim, S.E. Chung, S.-E. Choi, H. Lee, J. Kim, S. Kwon, Programming magnetic anisotropy in polymeric microactuators, Nat. Mater. 10 (2011) 747–752, https://doi.org/10.1038/nmat3090.
[33] Y. Alapan, A.C. Karacakol, S.N. Guzelhan, I. Isik, M. Sitti, Reprogrammable shape morphing of magnetic soft machines, Sci. Adv. 6 (2020) eabc6414, https://doi.org/10.1126/sciadv.abc6414.
[34] H. Deng, K. Sattari, Y. Xie, P. Liao, Z. Yan, J. Lin, Laser reprogramming magnetic anisotropy in soft composites for reconfigurable 3D shaping, Nat. Commun. 11 (2020) 6325, https://doi.org/10.1038/s41467-020-20229-6.
[35] R. Zhao, H. Dai, H. Yao, Liquid-Metal Magnetic Soft Robot With Reprogrammable Magnetization and Stiffness, IEEE Robot. Autom. Lett. 7 (2022) 4535–4541, https://doi.org/10.1109/LRA.2022.3151164.
[36] H. Song, H. Lee, J. Lee, J.K. Choe, S. Lee, J.Y. Yi, S. Park, J.-W. Yoo, M.S. Kwon, J. Kim, Reprogrammable Ferromagnetic Domains for Reconfigurable Soft Magnetic Actuators, Nano Lett. 20 (2020) 5185–5192, https://doi.org/10.1021/acs.nanolett.0c01418.
[37] G. Chen, B. Ma, J. Zhang, Y. Chen, H. Liu, Reprogrammable Magnetic Soft Robots Based on Low Melting Alloys, Adv. Intell. Syst. 5 (2023) 2300173, https://doi.org/10.1002/aisy.202300173.
[38] Z. Wang, L. Jing, K. Yao, Y. Yang, B. Zheng, C.M. Soukoulis, H. Chen, Y. Liu, Origami-Based Reconfigurable Metamaterials for Tunable Chirality, Adv. Mater. 29 (2017) 1700412, https://doi.org/10.1002/adma.201700412.
[39] T. Tachi, Rigid-Foldable Thick Origami, (n.d.).
[40] S.M. Sajadi, P.J. Boul, C. Thaemlitz, A.K. Meiyazhagan, A.B. Puthirath, C.S. Tiwary, M.M. Rahman, P.M. Ajayan, Direct Ink Writing of Cement Structures Modified with Nanoscale Additive, Adv. Eng. Mater. 21 (2019) 1801380, https://doi.org/10.1002/adem.201801380.
[41] R. Zhao, Y. Kim, S.A. Chester, P. Sharma, X. Zhao, Mechanics of hard-magnetic soft materials, J. Mech. Phys. Solids 124 (2019) 244–263, https://doi.org/10.1016/j.jmps.2018.10.008.
[42] Y. Zhang, C.J. Ng, Z. Chen, W. Zhang, S. Panjwani, K. Kowsari, H.Y. Yang, Q. Ge, Miniature Pneumatic Actuators for Soft Robots by High-Resolution Multimaterial 3D Printing, Adv. Mater. Technol. 4 (2019) 1900427, https://doi.org/10.1002/admt.201900427.
[43] P. Sun, J. Zhang, X. Zhu, H. Li, Y. Li, J. Yang, Z. Peng, G. Zhang, F. Wang, H. Lan, Directly Printed Interconnection Wires between Layers for 3D Integrated Stretchable Electronics, Adv. Mater. Technol. 7 (2022) 2200302, https://doi.org/10.1002/admt.202200302.
[44] X. Wan, L. Luo, Y. Liu, J. Leng, Direct Ink Writing Based 4D Printing of Materials and Their Applications, Adv. Sci. 7 (2020) 2001000, https://doi.org/10.1002/advs.202001000.
[45] Y. Jin, J. Liang, S. Wu, Y. Zhang, L. Zhou, Q. Wang, H. Liu, J. Zhu, Electrical Dynamic Switching of Magnetic Plasmon Resonance Based on Selective Lithium Deposition, Adv. Mater. 32 (2020) 2000058, https://doi.org/10.1002/adma.202000058.